

Part-aware Personalized Segment Anything Model for Patient-Specific Segmentation

Chenhui Zhao and Liyue Shen

Department of Electrical and Computer Engineering
University of Michigan, Ann Arbor, USA
{chuizhao,liyues}@umich.edu

Abstract. Precision medicine, such as patient-adaptive treatments utilizing medical images, poses new challenges for image segmentation algorithms due to (1) the large variability across different patients and (2) the limited availability of annotated data for each patient. In this work, we propose a data-efficient segmentation method to address these challenges, namely *Part-aware Personalized Segment Anything Model (P²SAM)*. Without any model fine-tuning, P²SAM enables seamless adaptation to any new patients relying only on one-shot patient-specific data. We introduce a novel part-aware prompt mechanism to select multiple-point prompts based on part-level features of the one-shot data. To further promote the robustness of the selected prompt, we propose a retrieval approach to handle outlier prompts. Extensive experiments demonstrate that P²SAM improves the performance by +8.0% and +2.0% mean Dice score within two patient-specific segmentation settings, and exhibits impressive generality across different application domains, *e.g.*, +6.4% mIoU on the PerSeg benchmark. Code will be released soon.

1 Introduction

Advances in modern precision medicine and healthcare have emphasized the importance of personalized treatment aiming at adapting to the specific patient [17]. For instance, in radiation therapy, patients undergoing multi-fraction treatment would benefit from longitudinal medical data analysis to timely adjust treatment planning specific to the individual patient [53]. To facilitate the treatment procedure, such analysis demands timely and accurate automatic segmentation of tumors and critical organs from medical images, which has underscored the role of computer vision approaches for the medical image segmentation task [1, 4, 21, 23]. Despite the great progress made by previous works [12, 22, 47, 52], their focus remains on improving segmentation accuracy within the standard paradigm: training on a large number of annotated images and evaluating on some validation samples. However, personalized treatment presents unique challenges for segmentation algorithms: (1) the large variability across different patients, and (2) the limited availability of annotated training data for each patient. Overcoming these obstacles requires a segmentation approach that can reliably generalize to different patients, in a data-efficient manner.

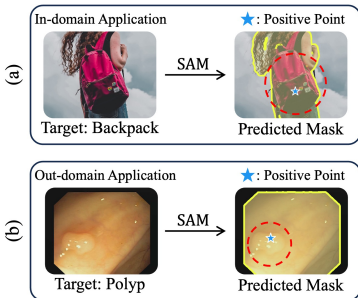


Fig. 1: Illustration of SAM’s ambiguity problem. The ground truth is circled by a red dashed circle, while the predicted mask is depicted by a yellow solid line.

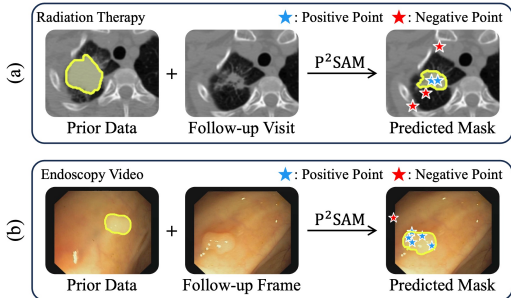


Fig. 2: Illustration of two patient-specific segmentation settings. P^2SAM can segment the follow-up data by utilizing the prior data as multiple-point prompts. The prior and predicted masks are depicted by a solid yellow line.

In this work, we address the unmet needs of the patient-specific segmentation by formulating it as an in-context segmentation problem, leveraging the promptable segmentation mechanism inherent in Segment Anything Model (SAM) [24]. Under this objective, our method seamlessly adapts to any new patients relying only on one-shot patient-specific prior data, without requiring additional training, thus in a data-efficient manner. To this end, we propose *Part-aware Personalized Segment Anything Model* (P^2SAM). For the original prompt mechanism of SAM, as illustrated by Fig. 1, a single-point prompt may result in ambiguous prediction, indicating the limitation in both in-domain and out-domain applications [20, 44, 64]. To alleviate the ambiguity problem, following the statement in SAM [24], "*ambiguity is much rarer with multiple prompts*", we propose a novel part-aware prompt mechanism to meticulously select multiple-point prompts based on part-level features of the one-shot prior data.

As illustrated in Fig. 2, our method enables reliable and robust adaptation to a new patient across various settings with one-shot prior data. Notably, Fig. 2 (b) demonstrates an example wherein P^2SAM addresses the ambiguity problem shown in Fig. 1. Specifically, we commence by clustering the prior data into multiple groups in the embedding space, for extracting part-level features. Then, we select multiple-point prompts based on the similarity between these part-level features and the follow-up data. While we employ SAM as the backbone method here, the proposed approach can be flexibly generalized to any promptable segmentation model that supports the point prompt as input.

On the other hand, as the number of parts increases, the chance of encountering outlier prompts may also increase. An extreme case is to cluster each image patch into different parts, which renders a lot of outlier prompts [38]. To make the part-aware prompt mechanism more robust, we introduced a retrieval approach to investigate the optimal number of parts required for each specific case. The retrieval approach is based on the distribution similarity between the foreground feature of the prior data and the result obtained under the current number of

parts. This approach is motivated by the fact that tumors and normal organs manifest in distinct distributions within medical imaging technologies [14].

With the aforementioned designs, P²SAM naturally resolves the ambiguity problem in the promptable segmentation method, demonstrating a robust generalization for both in-domain and out-domain applications using a simple yet effective method. The key contributions of this work lie in three-fold:

1. We propose a generic data-efficient segmentation method, namely P²SAM, enabling efficient and flexible adaptation to any specific settings, relying only on one-shot prior data, without any model fine-tuning.
2. We propose a novel part-aware prompt mechanism to meticulously select multiple-point prompts based on the part-level feature extraction with a distribution-based retrieval approach to filter outlier prompts, which effectively mitigates ambiguity and enhances the robust generalization capacity of any promptable segmentation models.
3. Our method largely benefits real-world applications like patient-specific segmentation, one-shot segmentation, and personalized segmentation. Experiment results demonstrate that P²SAM improves the performance by +8.0% and +2.0% mean Dice score in two patient-specific segmentation settings and achieves a new state-of-the-art result, *i.e.*, 95.7% mIoU on the personalized segmentation benchmark PerSeg.

2 Related Work

2.1 Segmentation Generalist

Over the past decade, various segmentation tasks including semantic segmentation [29, 40, 54], instance segmentation [16, 30–32], and panoptic segmentation [6, 9, 10, 37] have been extensively explored. Motivated by the success of foundational language models [5, 49, 50, 55], the computer vision research community is increasingly paying attention to developing more generalized or foundational models that can tackle various vision or multi-modal tasks [27, 28, 33, 34, 36, 48] through a unified model, or called foundation model [7, 15, 37, 46]. This has spurred several large-scale vision models [24, 59, 60, 62] for image segmentation. Notably, Segment Anything model (SAM) [24] introduces a promptable model architecture, including the positive- and negative-point prompt; the box prompt; and the mask prompt. SAM emerges with an impressive zero-shot interactive segmentation capability after pre-training on the large-scale SA-1B dataset [24]. Given the remarkable generalization capacity of SAM, researchers within the medical image field have been seeking to build a foundational model for medical image segmentation [63] upon SAM. While still worth further exploring, certain approaches [25, 42, 61] have already shown some promising results. For instance, MedSAM [42] has exhibited significant performance across various medical image segmentation tasks after fully fine-tuning SAM on an extensive medical dataset, however, its applicability remains constrained to the box prompt modality.

2.2 In-Context Learning

First introduced as a new paradigm in natural language processing [5], in-context learning allows the model to adapt to unseen input patterns with a few prompts and examples, without the need to fine-tune the model. Similar ideas [32, 51, 53] are also explored in other fields. For instance, in computer vision, few-shot segmentation [26, 39, 51, 58], like PANet [58], aims to segment new classes with only a few examples; in adaptive therapy [53], several works [8, 13, 56, 57] attempt to leverage limited patient-specific data to adapt to the specific patient case, but these methods still requires model fine-tuning in different manners.

Recent advancements, such as Painter [59] and SegGPT [60] pioneer novel in-context learning approaches for vision tasks, enabling the timely segmentation of images based on specified image-mask prompts. SEEM [65] further explores this concept by investigating different prompt modalities. More recently, PerSAM [64] and Matcher [38] have utilized SAM to tackle few-shot segmentation through the in-context learning fashion. PerSAM introduces a novel task, known as personalized object segmentation [64], which aims at adapting SAM to new views of a specific object. However, PerSAM prompts SAM with only a singular prompt, leading to the ambiguity problem in the segmentation results [24]. On the other hand, Matcher enhances segmentation accuracy by utilizing multiple sets of point prompts. However, Matcher’s prompt generation mechanism is based on patch-level features. This mechanism makes Matcher dependent on DI-NOv2 [46] to generate prompts, which is particularly pre-trained under a patch-level objective. Despite this, Matcher still generates a lot of outlier prompts. Thus, Matcher limitedly relies on a complicated framework and lacks flexibility and robustness when applied with other vision backbones, including SAM.

3 Method

We first introduce the problem setting within the context of patient-specific segmentation in Sec. 3.1. We introduce our proposed methodology, P²SAM, in Sec. 3.2. Note that our method can be applied to various application domains. Therefore, we incorporate natural image illustrations in this section to provide a more intuitive understanding. Finally, we present an optional fine-tuning strategy in Sec. 3.3, specifically designed to adapt the backbone method (SAM) to the medical image domain if required.

3.1 Problem Setting

Our method aims to adapt a promptable segmentation model to any new patients with one-shot patient-specific data, which can be obtained either from the initial visit to a hospital or the first frame of a medical video, as shown in Fig. 2. The prior data includes a reference image I_R and a mask M_R delineating the segmented object. Given a target image, I_T , our goal is to predict its mask M_T , without additional human annotation costs or model training burdens. This setting is also suitable for object-specific segmentation, where the target image represents a new view of the same object depicted in the prior data.

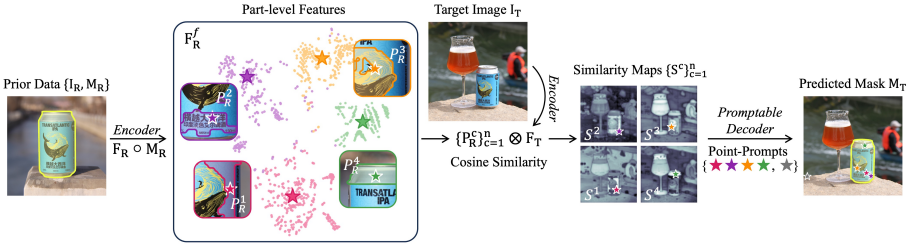


Fig. 3: Illustration of presenting the prior data in the form of multiple-point prompts. Masks are depicted by a yellow solid line. We first cluster foreground features in the reference image into part-level features. Then, we select multiple-point prompts based on the cosine similarity (\otimes in the figure) between these part-level features and target image features. A colorful star, matching the color of the corresponding part, denotes a positive-point prompt, while a gray star denotes a negative-point prompt. These prompts are subsequently fed into SAM’s promptable decoder to do prediction.

3.2 Methodology Overview

Part-aware Prompt Mechanism. To facilitate a clearer understanding of the significance of each part in our part-aware prompt mechanism, we illustrate this approach using a natural image, as shown in Fig. 3. We utilize SAM as the backbone method here, but our approach can be generalized to any other promptable segmentation models as long as they support the point prompt modality. Given the reference image-mask pair from the prior data, $\{I_R, M_R\}$, P²SAM first apply SAM’s *Encoder* to extract the visual features $F_R \in \mathbb{R}^{d \times h \times w}$ from the reference image I_R . Then, we utilize the reference mask M_R to select foreground features F_R^f according to:

$$F_R^f = F_R \circ M_R \quad (1)$$

where \circ represents the mask selection, $F_R^f \in \mathbb{R}^{d \times n_f}$, and n_f represents the number of foreground features. We further cluster F_R^f with k -mean++ [3] into n parts. Here, we showcase an example of $n=4$. We obtain the centroid of each part as the representative for the part-level features, by applying an average pooling, denoting as $\{P_R^c\}_{c=1}^n \in \mathbb{R}^{d \times n}$. For illustration, we align the features of each part in the feature space with pixels in the RGB space, thereby contouring the corresponding regions for each part in the image, respectively. We observe that SAM’s encoder tends to cluster features together based on texture features, such as the characters and images depicted on the can.

After that, we extract the features F_T from the target image I_T using SAM’s *Encoder* as well, and compute similarity maps $\{S^c\}_{c=1}^n \in \mathbb{R}^{n \times h \times w}$ based on the cosine similarity between the extracted part-level features $\{P_R^c\}_{c=1}^n$ and F_T by:

$$S^c_{ij} = \frac{P_R^c \cdot F_{Tij}}{\|P_R^c\|_2 \cdot \|F_{Tij}\|_2} \quad (2)$$

We determine n positive-point prompts $\{Pos^c\}_{c=1}^n$ with the highest similarity score on each similarity map S^c , depicted as colorful stars in Fig. 3.

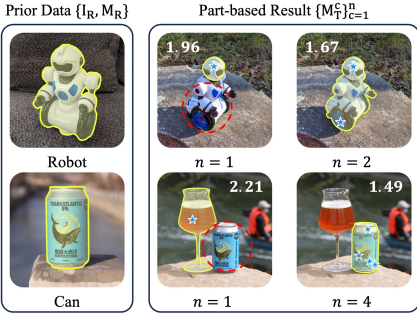


Fig. 4: Illustration of P²SAM’s improvement. A blue star represents the selected positive-point prompt.

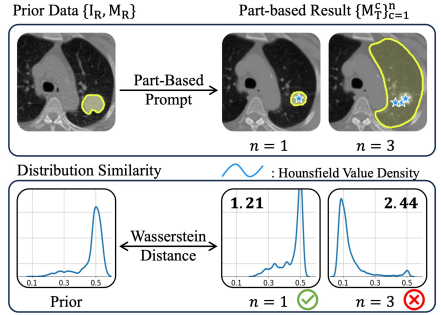


Fig. 5: Illustration of the proposed approach to retrieve the optimal number of parts for a specific case.

For natural images, the background of the reference image and the target image may exhibit little correlation. Thus, following the approach in PerSAM [64], we choose a negative-point prompt $\{Neg\}$ with the lowest score on the average similarity map $\frac{1}{n} \sum_{c=1}^n S^c$. $\{Neg\}$ is depicted as the gray star in Fig. 3. However, for medical images, the background of the reference image is highly correlated with the background of the target image, usually both representing normal anatomical structures. As a result, in medical images, shown as Fig. 2 in Sec. 1, we identify multiple negative-point prompts $\{Neg^c\}_{c=1}^n$ from the background. This procedure mirrors the selection of multiple positive-point prompts but we use background features F_R^b by replacing M_R with its logical negation \bar{M}_R in Eq. (1). Finally, we send both positive- and negative-point prompts into SAM’s *promptable decoder* and get the predicted mask for the target image M_T .

Retrieve the Optimal Number of Parts. The improvement of multiple-point prompts is illustrated in Fig. 4. The proposed approach can naturally avoid the ambiguous prediction introduced by SAM (*e.g.*, robot) and also improve precision (*e.g.*, can). However, this approach may occasionally result in outliers, as observed in the example of NSCLC segmentation in Fig. 5, $n=3$. Therefore, we propose a distribution-based retrieval approach to answer the question, “How many part-level features should we choose for a specific case?”. We assume the correct target foreground feature F_T^f ($F_T \circ M_T$), and the reference foreground feature F_R^f should belong to the same distribution. This assumption is grounded in the fact that tumors and normal organs will be reflected in distinct distributions by medical imaging technologies [14], also observed by the density of Hounsfield Unit value in Fig. 5. To retrieve the optimal number of parts for a specific case, we first set $\{1, \dots, n\}$ parts, and obtain n part-based target foreground features $\{\{F_T^f\}^c\}_{c=1}^n$. Following WGAN [2], we utilize Wasserstein distance to measure the distribution similarity between the reference foreground feature F_R^f and each target foreground feature $\{F_T^f\}^c$, to determine the final number of parts with the smallest distance. The smaller distance value for the correct prediction in Fig. 4 indicates this approach can also be extended to natural images.

3.3 Adapt SAM to Medical Image Domain with Fine-tuning

Segment Anything Model (SAM) [24] is initially pre-trained on the SA-1B [24] dataset in the natural image domain. Despite the scale of SA-1B, a notable domain gap persists between SA-1B and medical images. In more realistic medical scenarios, researchers may have access to certain public datasets [1, 23] tailored to specific applications, enabling them to fine-tune SAM. However, the fine-tuned SAM is still limited to generalizing across various medical data from different institutions because of the large variability in patient population, demographics, imaging protocol, etc., as mentioned in Sec. 1. Note that our proposed P²SAM can be flexibly plugged into the fine-tuned SAM model as well to improve robustness in these out-of-distribution testing cases. Specifically, in these medical scenarios, we initially utilize *in-distribution* datasets [1, 23] to fine-tune SAM. Then, we employ *out-distribution* datasets [4, 21] obtained from various institutions to mimic new patient scenarios. Note that there is no further fine-tuning on *out-distribution* datasets. In addition, we try both fully fine-tuning and a parameter-efficient fine-tuning method, Low-Rank adaptation (LoRA) [19], to further explore efficiency. During the fine-tuning process, to maintain the promptable ability of SAM, we adhere closely to the interactive training strategy [24] outlined in SAM. More details can be found in supplementary materials.

4 Experiments

We first introduce our experimental settings in Sec. 4.1. Then we evaluate our approach in Sec. 4.2 and show qualitative results in Sec. 4.3. Finally, we conducted several ablation studies to investigate our designs in Sec. 4.4. More results can be found in the supplementary materials.

4.1 Experiment Settings

Datasets. In our experiments, we utilize a total of four medical datasets, including two *in-distribution* datasets:

- The NSCLC-Radiomics dataset [1], collected for NSCLC segmentation, contains data from 422 patients. Each patient has a 3-dimensional computed tomography volume along with corresponding segmentation annotations.
- The Kvasir-SEG dataset [23], contains 1000 labeled polyp images, with different resolutions ranging from 332×487 to 1920×1072 .

and two *out-distribution* datasets from different institutions:

- The 4D-Lung dataset [21], collected for longitudinal analysis, contains data from 20 patients, within which 13 patients underwent multiple visits, 3 to 8 visits for each patient. For each visit, a 3-dimensional computed tomography volume along with corresponding segmentation labels is available.
- The CVC-ClinicDB dataset [4], contains 612 labeled polyp images selected from 29 endoscopy videos, with a resolution of 384×288 .

In-distribution datasets serve as the training dataset to adapt SAM to the medical domain, while *out-distribution* datasets serve as unseen patient cases.

Medical Scenarios and Challenges. For NSCLC segmentation in patient-adaptive radiation therapy, when deemed as a necessity, fine-tuning will be conducted on *in-distribution* dataset, NSCLC-Radiomics [1]. For P²SAM, experiments are then carried out on *out-distribution* dataset, 4D-Lung [21]. We evaluate P²SAM on patients who underwent multiple visits during treatment. For each patient, we utilize the image-mask pair from the first visit as the patient-specific prior data. For polyp segmentation in endoscopy video, fine-tuning will be conducted on *in-distribution* dataset, Kvasir-SEG [23]. Experiments for P²SAM are then carried out on *out-distribution* dataset, CVC-ClinicDB [4]. We evaluate P²SAM on 29 endoscopy videos. For each video, we utilize the image-mask pair from the first stable frame as the patient-specific prior data.

For NSCLC segmentation in patient-adaptive radiation therapy, the challenge arises from the variability in the patient’s position during each computed tomography scan throughout treatment, coupled with changes in the patient’s tumor anatomy throughout treatment. For polyp segmentation in endoscopy videos, the challenge stems from the discontinuity observed in endoscopy videos, where significant anatomical changes occur between adjacent frames.

Implementation Details. All experiments are conducted on A40 GPUs. In situations where fine-tuning is deemed necessary, for the NSCLC-Radiomics dataset [1], we extract 2-dimensional slices from the original computed tomography scans, resulting in a total of 7355 labeled images. For each image, we duplicate it along the channel dimension to match SAM’s input requirement. As for the Kvasir-SEG dataset [23], we utilize all 1000 labeled images. We process two datasets following existing works [12, 18]. Each dataset was randomly split into three subsets: training, validation, and testing, with an 80:10:10 percent ratio (patient-wise for the NSCLC-Radiomics dataset). The model is initialized with the pre-trained SAM model, and we also utilize the loss function proposed by SAM [24]. In the default setting, we optimize the model by AdamW optimizer ($\beta_1=0.9, \beta_2=0.999$) [41], with a weight decay of 0.05. We further penalize the SAM’s encoder [11] with a drop path of 0.1. We fine-tune the model for 36 epochs on the NSCLC-Radiomics dataset [1], and 100 epochs on the Kvasir-SEG dataset [23] with the batch size of 4. The initial learning rate is $1e-4$, and the fine-tuning process is guided by cosine learning rate decay, with a linear learning rate warm-up over the first 10 percent epochs.

In summary, we test P²SAM on *out-distribution* datasets with three different models: 1. original SA-1B [24] pre-trained SAM; 2. *in-distribution* datasets fine-tuned model with Low-Rank adaptation (LoRA) [19]; 3. *in-distribution* datasets fully fine-tuned model.

Baselines. We compare P²SAM against various methods, including previous approaches such as the *direct-transfer* baseline, fine-tuning on the prior information [8, 13, 56, 57], denoted as *fine-tune*, and PANet [58] for one-shot learning. Additionally, we include concurrent methods that also utilize SAM, such as PerSAM [64] and Matcher [38]. For PANet, we utilize its align method for one-shot segmentation. For Matcher, we adopt its setting of FSS-1000 [35]. It is important to note that all methods utilize the same SAM model for fairness.

Table 1: Results of NSCLC segmentation for patient-adaptive radiation therapy. We show the mean Dice score for each method. In situations where fine-tuning is deemed necessary, $base^{5.5M}$ indicates 5.5M trainable parameters in the SAM-base model. In addition, † indicates test-time training-free method; ‡ indicates the method using SAM.

Method	Original SAM	LoRA Fine-Tuned		Fully Fine-Tuned	
	$huge^{0.0M}$	$base^{5.5M}$	$large^{5.9M}$	$base^{93.8M}$	$large^{312.5M}$
<i>direct-transfer</i> [†]	-	56.10	57.83	58.18	61.11
<i>fine-tune</i>	-	52.11	32.55	55.27	53.85
PANet [†] [58]	4.28	5.24	7.79	40.03	44.70
Matcher ^{†‡} [38]	13.28	50.81	50.88	59.52	57.67
PerSAM ^{†‡} [64]	9.84	63.63	64.69	62.58	64.45
P ² SAM ^{†‡} (Ours)	28.52	64.38	67.00	66.68	67.23

4.2 Quantitative Results

Patient-Adaptive Radiation Therapy. As shown in Tab. 1, P²SAM outperforms all other baselines across various models. Notably, when directly utilizing original SAM, P²SAM can outperform Matcher by +15.24% and PerSAM by +18.68% mean Dice score. This highlights P²SAM’s superior adaptation to out-domain medical applications. In fine-tuning situations, P²SAM can outperform the *direct-transfer* baseline by +8.01% mean Dice score, surpassing recent methods that also use SAM: Matcher -3.59% and PerSAM +5.53% mean Dice score. This demonstrates that P²SAM can also enhance the model’s generalization capacity on the out-of-distribution application.

Within other methods, *fine-tune* is vulnerable to overfitting with one-shot data, resulting in failing to surpass even the *direct-transfer* baseline. Methods that heavily rely on the semantic representations of the model’s encoder also fail to surpass the *direct-transfer* baseline, such as PANet and Matcher. For PANet, this is due to its complete dependency on the encoder. For Matcher, the prompts selection is based on patch-level features, which can result in more outliers when the model is trained on limited medical data. Because of that, they are also not well-suited for parameter-efficient fine-tuning techniques as well and this susceptibility is much notable in PANet. PerSAM and our P²SAM, on the contrary, can help bridge the gap between parameter-efficient fine-tuning and fully fine-tuning. In some instances, these two methods with a parameter-efficient fine-tuned SAM can even surpass the results achieved by a fully fine-tuned SAM. P²SAM significantly mitigates the impact of ambiguity when employing the original SAM model. Moreover, when utilizing a fine-tuned model, where there is no ambiguity problem as described in supplementary material, P²SAM can still surpass PerSAM by providing more information to the promptable decoder.

Polyp Segmentation for Endoscopy Video. As shown in Tab. 2, P²SAM still outperforms all other methods across various models. When directly utilizing original SAM, P²SAM can outperform Matcher by +2.91% mean Dice score and

Table 2: Results of polyp segmentation for endoscopy video. We show the mean Dice score for each method. In situations where fine-tuning is deemed necessary, $base^{5.5M}$ indicates 5.5M trainable parameters in the SAM-base model. In addition, † indicates test-time training-free method; ‡ indicates the method using SAM.

Method	Original SAM	LoRA Fine-Tuned		Fully Fine-Tuned	
	$huge^{0.0M}$	$base^{5.5M}$	$large^{5.9M}$	$base^{93.8M}$	$large^{312.5M}$
direct-transfer†	-	77.20	81.16	84.62	86.68
fine-tune	-	75.29	79.50	83.14	86.67
PANet† [58]	38.22	44.61	55.48	75.99	86.48
Matcher†‡ [38]	63.54	78.65	79.56	85.17	87.15
PerSAM†‡ [64]	45.82	79.02	81.63	85.74	87.88
P ² SAM †‡ (Ours)	66.45	80.03	82.60	86.40	88.76

PerSAM by +20.63% mean Dice score. In fine-tuning situations, P²SAM can outperform the *direct-transfer* baseline by +2.03% mean Dice score, surpassing Matcher +0.22% mean Dice score and PerSAM +1.15% mean Dice score. Notably, P²SAM can achieve the new state-of-the-art result [12] for transferring Kvasir-SEG [23] pre-trained model on the CVC-ClinicDB [4] dataset.

Endoscopic videos are in RGB space, which tends to be less prone to overfitting issues compared to computed tomography images. Consequently, all methods exhibit enhanced performance in Tab. 2 when compared to Tab. 1. This is particularly evident for *fine-tune*, PANet, and Matcher. As SAM is pre-trained on an extensive dataset SA-1B [24], it possesses strong generalization capabilities. In datasets like CVC-ClinicDB [4], which exhibit a smaller domain gap [43] with the SA-1B [24], even the *direct-transfer* baseline demonstrates a state-of-the-art migration performance [12]. Hence, *fine-tune* and PANet still fail to surpass the *direct-transfer* performance. For Matcher, however, due to the improved semantic representation of the model’s encoder, its approach of selecting point prompts can result in fewer outliers. Consequently, it can surpass the *direct-transfer* baseline. When compared with PerSAM and our P²SAM, Matcher still lags behind because SAM’s semantic representation is not yet good enough to support its utilization of patch-level features for selecting point prompts. P²SAM outperforms PerSAM for the same aforementioned reasons: 1. by mitigating ambiguity when employing the original SAM; and 2. by offering additional information to the decoder when utilizing the fine-tuned model.

Existing One-shot Segmentation Benchmarks. To further demonstrate P²SAM’s generalization capacity in different application domains, we evaluate its performance on existing benchmarks, directly utilizing the original SAM. These benchmarks serve as in-domain out-of-distribution applications, including various one-shot semantic segmentation benchmarks, COCO-20ⁱ [45], FSS-1000 [35], LVIS-92ⁱ, and a personalized segmentation benchmark, PerSeg [64]. We follow previous works [38, 64] for data pre-processing and evaluation.

Table 3: Results of one-shot semantic segmentation on COCO-20ⁱ, FSS-1000, LVIS-92ⁱ, and PerSeg. † indicates the training-free method. ‡ indicates the method using SAM. Gray indicates in-distribution datasets trained model. Note that Matcher utilizes SAM’s encoder for fairness.

Method	COCO-20 ⁱ [45]	FSS-1000 [35]	LVIS-92 ⁱ [38]	PerSeg [35]
Painter [59]	33.1	61.7	10.5	56.4
SegGPT [60]	56.1	85.6	18.6	94.3
SEEM [65]	-	-	-	87.1
Matcher ^{†‡} [38]	25.1	82.1	12.6	90.2
PerSAM ^{†‡} [64]	23.0	71.2	11.5	89.3
PerSAM-F [‡] [64]	23.5	75.6	12.3	95.3
P ² SAM ^{†‡} (Ours)	26.0	82.4	13.7	95.7

In Tab. 3, when directly utilizing SAM’s encoder, P²SAM outperforms concurrent works, Matcher, PerSAM, and PerSAM’s fine-tuned version PerSAM-F on all existing benchmarks. P²SAM consistently exhibits an advantage over PerSAM and PerSAM-F. This is because our part-aware prompt mechanism not only naturally addresses the ambiguity problem but also enhances prompts’ accuracy. Furthermore, we also slightly surpassed Matcher. This is because our prompts selection method is based on part-level features, which is more robust compared to selecting prompts based on patch-level features. P²SAM can outperform Painter [59] on two difficult datasets, FSS-1000 [35] and LVIS-92ⁱ [38], demonstrating the generality of our method. Although still lagging behind SegGPT [60], akin to Matcher, our method is entirely training-free during testing, making it more efficient. In addition, P²SAM can achieve a new state-of-the-art result on the personalized segmentation benchmark, PerSeg [64], which is a close scenario to patient-specific segmentation. This achievement further demonstrates the generalization capacity of our method on personalized and patient-specific segmentation.

4.3 Qualitative Result

To illustrate how P²SAM enhances the generalization capacity of a promptable segmentation model for both in-domain and out-domain applications, we visualize the qualitative segmentation results in patient-adaptive radiation therapy and endoscopy videos. As shown in Fig. 6 and Fig. 7, when directly utilizing the original SAM model, our P²SAM can achieve higher-quality masks than Matcher and PerSAM. In Fig. 6, P²SAM’s success comes from our thorough exploration of SAM’s prompt mechanism. By presenting a large number of negative-point prompts, we enforce the model’s focus on the semantic target. Results in Fig. 7 further corroborate the benefits of our method: unambiguous segmentation and robust prompts selection. When utilizing the model fine-tuned on the *out-distribution* medical dataset, our P²SAM can also enhance in-domain

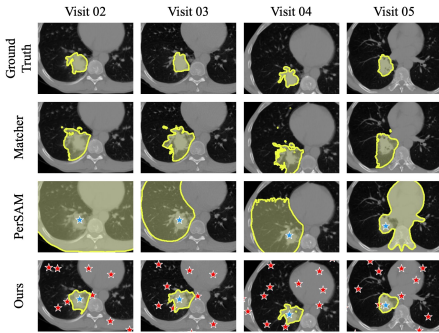


Fig. 6: Qualitative results of NSCLC segmentation on the 4D-Lung dataset, with original SAM model.

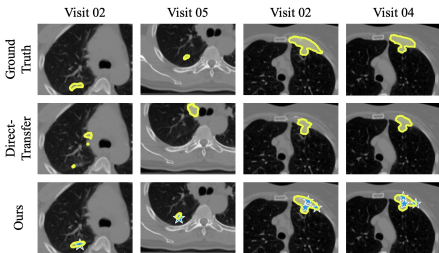


Fig. 8: Qualitative results of NSCLC segmentation from two patients on the 4D-Lung dataset, with the fine-tuned model.

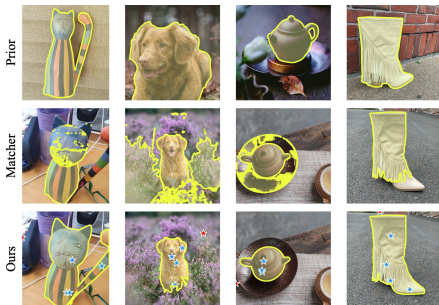


Fig. 10: Qualitative results of personalized segmentation on the PerSeg dataset, compared with Matcher.

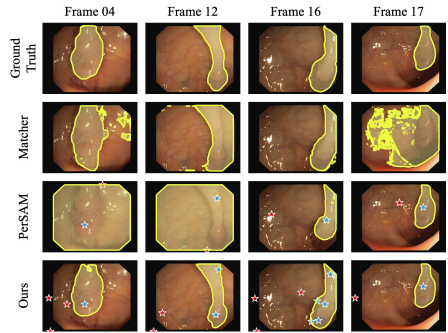


Fig. 7: Qualitative results of polyp segmentation on the CVC-ClinicDB dataset, with original SAM model.

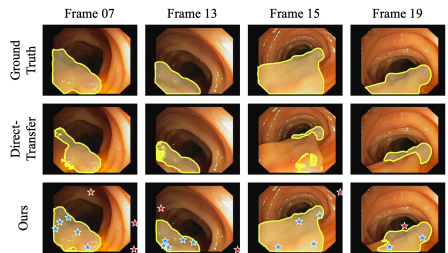


Fig. 9: Qualitative results of polyp segmentation on the CVC-ClinicDB dataset, with the fine-tuned model.

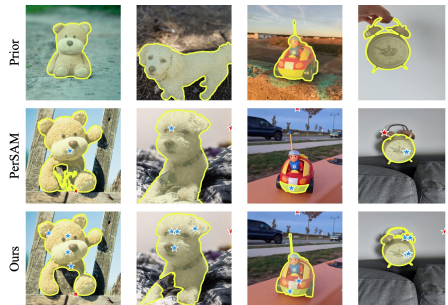


Fig. 11: Qualitative results of personalized segmentation on the PerSeg dataset, compared with PerSAM.

generality by providing accurate foreground information when the object is too small, as shown in the first two columns of Fig. 8, and additional foreground information when the segmentation is incomplete, as shown in the last second two columns of Fig. 8 and Fig. 9. We illustrate the qualitative results of personalized segmentation on PerSeg in Fig. 10 and Fig. 11, compared with Matcher [38] and PerSAM [64] respectively. The remarkable results demonstrate that P²SAM can generalize well to different domain applications.

Table 4: Ablation study for the number of parts n and the retrieval approach. Default settings are marked in Gray .

# parts (n)	CVC-ClinicDB (mean Dice)		PerSeg (mean IoU)	
	<i>w/o</i> retrieval	<i>w/</i> retrieval	<i>w/o</i> retrieval	<i>w/</i> retrieval
1 (PerSAM)	45.8	45.8	89.3	89.3
2	53.9	59.5	83.7	92.9
3	53.6	61.9	91.0	95.6
4	54.3	63.1	93.8	95.6
5	56.6	64.2	93.3	95.7

Table 5: Ablation study for the distribution similarity measurement. Default settings are marked in Gray .

Algorithm	CVC-ClinicDB	PerSeg
<i>w/o retrieval</i>	54.3	93.8
<i>Hungarian</i>	61.1	95.6
<i>Jensen-Shannon</i>	58.1	94.0
<i>Wasserstein</i>	63.1	95.6

Table 6: Ablation study for different model sizes. Default settings are marked in Gray .

Model	CVC-ClinicDB	PerSeg
PerSAM ^{huge}	45.8	89.3
SAM-base	55.1	90.0 _{26.0/2.8} ↑
SAM-large	63.8	95.6 _{9.0/3.4} ↑
SAM-huge	63.1	95.6 _{6.3/0.3} ↑

4.4 Ablation Study

In this section, we utilize the original SAM model for all experiments. Ablation studies are conducted on the in-domain PerSeg dataset [64] and the out-domain CVC-ClinicDB dataset [4]. We explore the effects of the number of parts in the part-aware prompt mechanism, the retrieval approach, different measurements in the retrieval approach, and the model size.

Number of Parts n . To validate the efficacy of the part-aware prompt mechanism, we establish a method without the retrieval approach. As shown in Tab. 4, for both datasets, even solely relying on the part-aware prompt mechanism, increasing the number of parts n enhances segmentation performance. When setting $n=5$, our part-aware prompt mechanism enhances performance by +10.7% mean Dice score on CVC-ClinicDB, +4.0% mean IoU score on PerSeg. These substantial improvements underscore the effectiveness of our part-aware prompt mechanism to augment the generality of a promptable segmentation model across both in-domain and out-domain applications.

Retrieval Approach. Further validation of the effectiveness of our retrieval approach is also presented in Tab. 4. Utilizing the retrieval approach consistently yields improvements on both datasets. Note that, this approach is more effective on the CVC-ClinicDB dataset compared to the PerSeg dataset. This discrepancy can be attributed to the higher likelihood of inappropriate prompts occurring in out-domain applications. When setting $n=5$, our retrieval approach enhances

performance by +7.6% mean Dice score on CVC-ClinicDB, +2.4% mean IoU score on PerSeg. These substantial improvements show that our retrieval approach can retrieve an appropriate number of parts for different cases. The effectiveness of our retrieval approach suggests that we can initially set a wide range of parts for retrieval in the implementation. For the following experiments, we will set $n=4$.

Distribution Similarity Measurements. The cornerstone of our retrieval approach lies in distribution similarity measurements. To evaluate the efficacy of various algorithms, in Tab. 5, we juxtapose two distribution-related algorithms, namely Wasserstein distance and Jensen–Shannon divergence, alongside a feature matching algorithm, Hungarian bipartite matching. After obtaining two sets of foreground features from the reference image and the target image, we compute Wasserstein distance following the principles of WGAN [2]. Additionally, we calculate the Jensen-Shannon divergence based on the first two principal components of each feature. Regarding the feature-matching algorithm, we initially cluster these two sets of features into an equal number of clusters. Subsequently, we compute the mean cosine similarity across these cluster centers based on Hungarian bipartite matching. All algorithms exhibit improvements in segmentation performance compared to the *w/o retrieval* baseline, while the Wasserstein distance is better in our context. The efficacy of the Jensen-Shannon divergence further corroborates our assumption that foreground features from the reference image and a correct target result should align in the same distribution, albeit it faces challenges when handling high-dimensional data formats.

Model Size. In Tab. 6, we investigate the performance of other model sizes for our P²SAM, *i.e.*, SAM-base, SAM-large, and SAM-huge. As shown, for CVC-ClinicDB, a larger model size does not necessarily lead to better results. This result aligns with current conclusions [20, 44], in medical image analysis, the SAM-huge model may occasionally be outperformed by the SAM-large model. On the other hand, for the PerSeg dataset, even utilizing the SAM-base model, P²SAM achieves higher accuracy compared to PerSAM with a SAM-huge model. Additionally, alongside P²SAM’s results, we show the improvement over PerSAM and PerSAM-F under the same model size. These findings further underscore the robustness of P²SAM, particularly in scenarios where the model exhibits weaker representation, a circumstance more prevalent in medical image analysis.

5 Conclusion

In this paper, we pioneer a solution to patient-specific segmentation by formulating it as an in-context segmentation problem. We propose a generic segmentation model, P²SAM, to effectively integrate prior information into current segmentation tasks. P²SAM comprises a novel part-aware prompt mechanism and a distribution-based retrieval approach to filter outlier prompts. These two components effectively mitigate ambiguity and enhance the robust generalization capacity of any promptable segmentation models. We hope our work may expand the applicability of SAM to a wider range of medical scenarios.

References

1. Aerts, H., Velazquez, E.R., Leijenaar, R., Parmar, C., Grossmann, P., Cavalho, S., Bussink, J., Monshouwer, R., Haibe-Kains, B., Rietveld, D., et al.: Data from nscic-radiomics. The cancer imaging archive (2015) **1**, **7**, **8**
2. Arjovsky, M., Chintala, S., Bottou, L.: Wasserstein generative adversarial networks. In: International conference on machine learning. pp. 214–223. PMLR (2017) **6**, **14**
3. Arthur, D., Vassilvitskii, S., et al.: k-means++: The advantages of careful seeding. In: Soda. vol. 7, pp. 1027–1035 (2007) **5**
4. Bernal, J., Sánchez, F.J., Fernández-Esparrach, G., Gil, D., Rodríguez, C., Vilar-iño, F.: Wm-dova maps for accurate polyp highlighting in colonoscopy: Validation vs. saliency maps from physicians. *Computerized medical imaging and graphics* **43**, 99–111 (2015) **1**, **7**, **8**, **10**, **13**
5. Brown, T., Mann, B., Ryder, N., Subbiah, M., Kaplan, J.D., Dhariwal, P., Neelakantan, A., Shyam, P., Sastry, G., Askell, A., et al.: Language models are few-shot learners. *Advances in neural information processing systems* **33**, 1877–1901 (2020) **3**, **4**
6. Carion, N., Massa, F., Synnaeve, G., Usunier, N., Kirillov, A., Zagoruyko, S.: End-to-end object detection with transformers. In: European conference on computer vision. pp. 213–229. Springer (2020) **3**
7. Caron, M., Touvron, H., Misra, I., Jégou, H., Mairal, J., Bojanowski, P., Joulin, A.: Emerging properties in self-supervised vision transformers. In: Proceedings of the IEEE/CVF international conference on computer vision. pp. 9650–9660 (2021) **3**
8. Chen, Y., Gensheimer, M.F., Bagshaw, H.P., Butler, S., Yu, L., Zhou, Y., Shen, L., Kovalchuk, N., Surucu, M., Chang, D.T., et al.: Patient-specific auto-segmentation on daily kvct images for adaptive radiotherapy. *International Journal of Radiation Oncology* Biology* Physics* (2023) **4**, **8**
9. Cheng, B., Choudhuri, A., Misra, I., Kirillov, A., Girdhar, R., Schwing, A.G.: Mask2former for video instance segmentation. arXiv preprint arXiv:2112.10764 (2021) **3**
10. Cheng, B., Schwing, A., Kirillov, A.: Per-pixel classification is not all you need for semantic segmentation. *Advances in Neural Information Processing Systems* **34**, 17864–17875 (2021) **3**
11. Dosovitskiy, A., Beyer, L., Kolesnikov, A., Weissenborn, D., Zhai, X., Unterthiner, T., Dehghani, M., Minderer, M., Heigold, G., Gelly, S., et al.: An image is worth 16x16 words: Transformers for image recognition at scale. arXiv preprint arXiv:2010.11929 (2020) **8**
12. Dumitru, R.G., Peteleaza, D., Craciun, C.: Using duck-net for polyp image segmentation. *Scientific Reports* **13**(1), 9803 (2023) **1**, **8**, **10**
13. Elmahdy, M.S., Ahuja, T., van der Heide, U.A., Staring, M.: Patient-specific fine-tuning of deep learning models for adaptive radiotherapy in prostate ct. In: 2020 IEEE 17th International Symposium on Biomedical Imaging (ISBI). pp. 577–580. IEEE (2020) **4**, **8**
14. García-Figueiras, R., Baleato-González, S., Padhani, A.R., Luna-Alcalá, A., Vallejo-Casas, J.A., Sala, E., Vilanova, J.C., Koh, D.M., Herranz-Carnero, M., Vargas, H.A.: How clinical imaging can assess cancer biology. *Insights into imaging* **10**, 1–35 (2019) **3**, **6**
15. He, K., Chen, X., Xie, S., Li, Y., Dollár, P., Girshick, R.: Masked autoencoders are scalable vision learners. In: Proceedings of the IEEE/CVF conference on computer vision and pattern recognition. pp. 16000–16009 (2022) **3**

16. He, K., Gkioxari, G., Dollár, P., Girshick, R.: Mask r-cnn. In: Proceedings of the IEEE international conference on computer vision. pp. 2961–2969 (2017) **3**
17. Hodson, R.: Precision medicine. *Nature* **537**(7619), S49–S49 (2016) **1**
18. Hossain, S., Najeeb, S., Shahriyar, A., Abdullah, Z.R., Ariful Haque, M.: A pipeline for lung tumor detection and segmentation from ct scans using dilated convolutional neural networks. In: ICASSP 2019 - 2019 IEEE International Conference on Acoustics, Speech and Signal Processing (ICASSP). pp. 1348–1352 (2019). <https://doi.org/10.1109/ICASSP.2019.8683802> **8**
19. Hu, E.J., Shen, Y., Wallis, P., Allen-Zhu, Z., Li, Y., Wang, S., Wang, L., Chen, W.: Lora: Low-rank adaptation of large language models. arXiv preprint arXiv:2106.09685 (2021) **7, 8**
20. Huang, Y., Yang, X., Liu, L., Zhou, H., Chang, A., Zhou, X., Chen, R., Yu, J., Chen, J., Chen, C., et al.: Segment anything model for medical images? *Medical Image Analysis* **92**, 103061 (2024) **2, 14**
21. Hugo, G.D., Weiss, E., Sleeman, W.C., Balik, S., Keall, P.J., Lu, J., Williamson, J.F.: Data from 4d lung imaging of nslc patients. *The Cancer Imaging Archive* **10**, K9 (2016) **1, 7, 8**
22. Isensee, F., Jaeger, P.F., Kohl, S.A., Petersen, J., Maier-Hein, K.H.: nnu-net: a self-configuring method for deep learning-based biomedical image segmentation. *Nature methods* **18**(2), 203–211 (2021) **1**
23. Jha, D., Smedsrud, P.H., Riegler, M.A., Halvorsen, P., de Lange, T., Johansen, D., Johansen, H.D.: Kvasir-seg: A segmented polyp dataset. In: MultiMedia Modeling: 26th International Conference, MMM 2020, Daejeon, South Korea, January 5–8, 2020, Proceedings, Part II 26. pp. 451–462. Springer (2020) **1, 7, 8, 10**
24. Kirillov, A., Mintun, E., Ravi, N., Mao, H., Rolland, C., Gustafson, L., Xiao, T., Whitehead, S., Berg, A.C., Lo, W.Y., et al.: Segment anything. arXiv preprint arXiv:2304.02643 (2023) **2, 3, 4, 7, 8, 10**
25. Lei, W., Wei, X., Zhang, X., Li, K., Zhang, S.: Medlsam: Localize and segment anything model for 3d medical images. arXiv preprint arXiv:2306.14752 (2023) **3**
26. Leng, T., Zhang, Y., Han, K., Xie, X.: Self-sampling meta sam: Enhancing few-shot medical image segmentation with meta-learning. In: Proceedings of the IEEE/CVF Winter Conference on Applications of Computer Vision. pp. 7925–7935 (2024) **4**
27. Li, X., Cao, H., Zhao, S., Li, J., Zhang, L., Raj, B.: Panoramic video salient object detection with ambisonic audio guidance. In: Proceedings of the AAAI Conference on Artificial Intelligence. vol. 37, pp. 1424–1432 (2023) **3**
28. Li, X., Chen, Y., Lin, C.C., Singh, R., Raj, B., Liu, Z.: Completing visual objects via bridging generation and segmentation. arXiv preprint arXiv:2310.00808 (2023) **3**
29. Li, X., Lin, C.C., Chen, Y., Liu, Z., Wang, J., Raj, B.: Paintseg: Training-free segmentation via painting. arXiv preprint arXiv:2305.19406 (2023) **3**
30. Li, X., Wang, J., Li, X., Lu, Y.: Hybrid instance-aware temporal fusion for online video instance segmentation. In: Proceedings of the AAAI Conference on Artificial Intelligence. vol. 36, pp. 1429–1437 (2022) **3**
31. Li, X., Wang, J., Li, X., Lu, Y.: Video instance segmentation by instance flow assembly. *IEEE Transactions on Multimedia* (2022) **3**
32. Li, X., Wang, J., Xu, X., Li, X., Raj, B., Lu, Y.: Robust referring video object segmentation with cyclic structural consensus. In: Proceedings of the IEEE/CVF International Conference on Computer Vision. pp. 22236–22245 (2023) **3, 4**
33. Li, X., Wang, J., Xu, X., Peng, X., Singh, R., Lu, Y., Raj, B.: Towards robust audiovisual segmentation in complex environments with quantization-based semantic decomposition. arXiv preprint arXiv:2310.00132 (2023) **3**

34. Li, X., Wang, J., Xu, X., Yang, M., Yang, F., Zhao, Y., Singh, R., Raj, B.: Towards noise-tolerant speech-referring video object segmentation: Bridging speech and text. In: Proceedings of the 2023 Conference on Empirical Methods in Natural Language Processing. pp. 2283–2296 (2023) [3](#)
35. Li, X., Wei, T., Chen, Y.P., Tai, Y.W., Tang, C.K.: Fss-1000: A 1000-class dataset for few-shot segmentation. In: Proceedings of the IEEE/CVF conference on computer vision and pattern recognition. pp. 2869–2878 (2020) [8](#), [10](#), [11](#)
36. Li, X., Wen, Y., Yang, M., Wang, J., Singh, R., Raj, B.: Rethinking voice-face correlation: A geometry view. In: Proceedings of the 31st ACM International Conference on Multimedia. pp. 2458–2467 (2023) [3](#)
37. Li, Y., Mao, H., Girshick, R., He, K.: Exploring plain vision transformer backbones for object detection. In: European Conference on Computer Vision. pp. 280–296. Springer (2022) [3](#)
38. Liu, Y., Zhu, M., Li, H., Chen, H., Wang, X., Shen, C.: Matcher: Segment anything with one shot using all-purpose feature matching. arXiv preprint arXiv:2305.13310 (2023) [2](#), [4](#), [8](#), [9](#), [10](#), [11](#), [12](#)
39. Liu, Y., Zhang, X., Zhang, S., He, X.: Part-aware prototype network for few-shot semantic segmentation. In: Computer Vision—ECCV 2020: 16th European Conference, Glasgow, UK, August 23–28, 2020, Proceedings, Part IX 16. pp. 142–158. Springer (2020) [4](#)
40. Long, J., Shelhamer, E., Darrell, T.: Fully convolutional networks for semantic segmentation. In: Proceedings of the IEEE conference on computer vision and pattern recognition. pp. 3431–3440 (2015) [3](#)
41. Loshchilov, I., Hutter, F.: Decoupled weight decay regularization. arXiv preprint arXiv:1711.05101 (2017) [8](#)
42. Ma, J., He, Y., Li, F., Han, L., You, C., Wang, B.: Segment anything in medical images. *Nature Communications* **15**(1), 654 (2024) [3](#)
43. Matsoukas, C., Haslum, J.F., Sorkhei, M., Söderberg, M., Smith, K.: What makes transfer learning work for medical images: Feature reuse & other factors. In: Proceedings of the IEEE/CVF Conference on Computer Vision and Pattern Recognition. pp. 9225–9234 (2022) [10](#)
44. Mazurowski, M.A., Dong, H., Gu, H., Yang, J., Konz, N., Zhang, Y.: Segment anything model for medical image analysis: an experimental study. *Medical Image Analysis* **89**, 102918 (2023) [2](#), [14](#)
45. Nguyen, K., Todorovic, S.: Feature weighting and boosting for few-shot segmentation. In: Proceedings of the IEEE/CVF International Conference on Computer Vision. pp. 622–631 (2019) [10](#), [11](#)
46. Oquab, M., Darcet, T., Moutakanni, T., Vo, H., Szafraniec, M., Khalidov, V., Fernandez, P., Haziza, D., Massa, F., El-Nouby, A., et al.: Dinov2: Learning robust visual features without supervision. arXiv preprint arXiv:2304.07193 (2023) [3](#), [4](#)
47. Primakov, S.P., Ibrahim, A., van Timmeren, J.E., Wu, G., Keek, S.A., Beauque, M., Granzier, R.W., Lavrova, E., Scrivener, M., Sanduleanu, S., et al.: Automated detection and segmentation of non-small cell lung cancer computed tomography images. *Nature communications* **13**(1), 3423 (2022) [1](#)
48. Qu, L., Zou, X., Li, X., Wen, Y., Singh, R., Raj, B.: The hidden dance of phonemes and visage: Unveiling the enigmatic link between phonemes and facial features. arXiv preprint arXiv:2307.13953 (2023) [3](#)
49. Radford, A., Narasimhan, K., Salimans, T., Sutskever, I., et al.: Improving language understanding by generative pre-training (2018) [3](#)
50. Radford, A., Wu, J., Child, R., Luan, D., Amodei, D., Sutskever, I., et al.: Language models are unsupervised multitask learners. *OpenAI blog* **1**(8), 9 (2019) [3](#)

51. Rakelly, K., Shelhamer, E., Darrell, T., Efros, A., Levine, S.: Conditional networks for few-shot semantic segmentation (2018) [4](#)
52. Ronneberger, O., Fischer, P., Brox, T.: U-net: Convolutional networks for biomedical image segmentation. In: Medical Image Computing and Computer-Assisted Intervention—MICCAI 2015: 18th International Conference, Munich, Germany, October 5–9, 2015, Proceedings, Part III 18. pp. 234–241. Springer (2015) [1](#)
53. Sonke, J.J., Aznar, M., Rasch, C.: Adaptive radiotherapy for anatomical changes. In: Seminars in radiation oncology. vol. 29, pp. 245–257. Elsevier (2019) [1](#), [4](#)
54. Strudel, R., Garcia, R., Laptev, I., Schmid, C.: Segmenter: Transformer for semantic segmentation. In: Proceedings of the IEEE/CVF international conference on computer vision. pp. 7262–7272 (2021) [3](#)
55. Touvron, H., Lavril, T., Izacard, G., Martinet, X., Lachaux, M.A., Lacroix, T., Rozière, B., Goyal, N., Hambro, E., Azhar, F., et al.: Llama: Open and efficient foundation language models. arXiv preprint arXiv:2302.13971 (2023) [3](#)
56. Wang, C., Alam, S.R., Zhang, S., Hu, Y.C., Nadeem, S., Tyagi, N., Rimmer, A., Lu, W., Thor, M., Zhang, P.: Predicting spatial esophageal changes in a multimodal longitudinal imaging study via a convolutional recurrent neural network. *Physics in Medicine & Biology* **65**(23), 235027 (2020) [4](#), [8](#)
57. Wang, C., Tyagi, N., Rimmer, A., Hu, Y.C., Veeraraghavan, H., Li, G., Hunt, M., Mageras, G., Zhang, P.: Segmenting lung tumors on longitudinal imaging studies via a patient-specific adaptive convolutional neural network. *Radiotherapy and Oncology* **131**, 101–107 (2019) [4](#), [8](#)
58. Wang, K., Liew, J.H., Zou, Y., Zhou, D., Feng, J.: Panet: Few-shot image semantic segmentation with prototype alignment. In: proceedings of the IEEE/CVF international conference on computer vision. pp. 9197–9206 (2019) [4](#), [8](#), [9](#), [10](#)
59. Wang, X., Wang, W., Cao, Y., Shen, C., Huang, T.: Images speak in images: A generalist painter for in-context visual learning. In: Proceedings of the IEEE/CVF Conference on Computer Vision and Pattern Recognition. pp. 6830–6839 (2023) [3](#), [4](#), [11](#)
60. Wang, X., Zhang, X., Cao, Y., Wang, W., Shen, C., Huang, T.: Seggpt: Segmenting everything in context. arXiv preprint arXiv:2304.03284 (2023) [3](#), [4](#), [11](#)
61. Wu, J., Fu, R., Fang, H., Liu, Y., Wang, Z., Xu, Y., Jin, Y., Arbel, T.: Medical sam adapter: Adapting segment anything model for medical image segmentation. arXiv preprint arXiv:2304.12620 (2023) [3](#)
62. Yan, B., Jiang, Y., Wu, J., Wang, D., Luo, P., Yuan, Z., Lu, H.: Universal instance perception as object discovery and retrieval. In: Proceedings of the IEEE/CVF Conference on Computer Vision and Pattern Recognition. pp. 15325–15336 (2023) [3](#)
63. Zhang, L., Deng, X., Lu, Y.: Segment anything model (sam) for medical image segmentation: A preliminary review. In: 2023 IEEE International Conference on Bioinformatics and Biomedicine (BIBM). pp. 4187–4194. IEEE (2023) [3](#)
64. Zhang, R., Jiang, Z., Guo, Z., Yan, S., Pan, J., Dong, H., Gao, P., Li, H.: Personalize segment anything model with one shot. arXiv preprint arXiv:2305.03048 (2023) [2](#), [4](#), [6](#), [8](#), [9](#), [10](#), [11](#), [12](#), [13](#)
65. Zou, X., Yang, J., Zhang, H., Li, F., Li, L., Wang, J., Wang, L., Gao, J., Lee, Y.J.: Segment everything everywhere all at once. *Advances in Neural Information Processing Systems* **36** (2024) [4](#), [11](#)